Many-body effects in the population dynamics of terahertz quantum cascade lasers

F. Wang, X. G. Guo, and J. C. Cao*

State Key Laboratory of Functional Materials for Informatics, Shanghai Institute of Microsystem and Information Technology, Chinese Academy of Sciences, 865 Changning Road, Shanghai 200050, China

(Received 15 July 2009; revised manuscript received 10 November 2009; published 12 January 2010)

The time-dependent population inversions induced by ultrafast 2π and π pulses are simulated by cascade effective Bloch equations in terahertz quantum cascade lasers. The effective nonlinear chirped π pulse is used to achieve the Rabi flopping of population inversion and the oscillations in recovery process are found. With nonchirped pulse, we demonstrate that the oscillations in recovery process and the shift of resonant pump frequency are rooted from the many-body effects of the polarization. With a short dephasing time, the population changes are similar with the results of rate-equation model.

DOI: 10.1103/PhysRevB.81.045308 PACS number(s): 73.63.−b, 42.65.−k, 73.21.Cd, 78.20.Bh

I. INTRODUCTION

The quantum cascade laser (QCL) has been widely studied as an important device of lasing in mid-infrared region or far-infrared region.[1–3] The terahertz QCL can be used in medical and environmental detection, wireless communication, etc. In the quantum cascade structure, population inversion is achieved by the special tailoring of the quantum structure that can control the intersubband scattering lifetimes and the electrons transport into the upper lasing state by scattering and resonant tunneling through an injection barrier. The pump-probe method is an important tool of investigating the coherent transport of electrons through the cascade structures.[4,5] This experimental method is helpful to our research in the physical mechanism of population dynamics in the terahertz QCL and some theoretical works have been done by Weber *et al.*[6] Recently, femtosecond pump-probe experiments on an operating mid-infrared QCL have been done by Choi *et al.*[7,8] In this experiment, the phenomena of photon-driven transport and gain recovery have been studied experimentally and theoretically. In their theoretical work, the rate-equation method has been used to simulate the population dynamics of the quantum cascade structure.

At present, mostly, there are three methods used in the simulation of electron transport in quantum cascade structures: rate equation, Monte Carlo (MC) simulation, and semiconductor Bloch equations (SBEs). The rate equation and MC simulation have been used to analyze the electron transport in mid-infrared QCL and terahertz QCL (Refs. 9 and 10) but these two methods cannot work when we consider the coherent effects in the system. The SBEs are a helpful approach to simulate the dynamics of electrons when the device is pumped by an intense laser field.[6,11–13] Within this approach, we can study the coherent effects between the resonant levels clearly. But it is difficult to use SBEs practically, especially in the quantum cascade structure, because the computational complexity is too large and it is hard to include the electron-electron interaction which is important in the terahertz QCL. Recently, the coherent nonlinear optical phenomena in intersubband transitions in GaAs/AlGaAs coupled quantum wells have been studied by using the effective Bloch equations which derived from the SBEs with the averaging method by Batista *et al.*[14] and Olaya-Castro *et al.*[15] These simpler equations have been widely used and many interesting effects have been studied, such as instantaneous effect and many-body effects.[16–18] To the best of our knowledge, the many-body effects with ultrafast pulse in terahertz QCL have not been studied.

In this paper, we focus on the role of many-body effects in coherent polarization induced by 2π and π pulses. We neglect the polarization of the tunneling process to magnify the effects. In order to achieve this point, we apply a terahertz QCL based on a three-well active module as our research object. We extend the effective Bloch equations by appending a cascade term so they can be used in the terahertz QCL. We approximately use the scattering rates derived from the results of MC simulation in the stationary state. At last, we derive the numerical results with different pulses and dephasing times from the cascade effective Bloch equations. We represent some interesting phenomena that have never been found and then the importance of the many-body effects is demonstrated.

II. CASCADE EFFECTIVE BLOCH EQUATIONS TO TERAHERTZ QUANTUM CASCADE LASERS

In order to make a clear analogy and provide a vivid picture, we focus on the terahertz QCL based on a three-well active module which was first realized by Liu and co-workers.[19] The diagram of the calculated band structure of the terahertz QCL is shown in Fig. 1. The device was fabricated and processed in 1 mm long and 100 μm wide. The design bias is 14.4 kV/cm. It is operating at 3.4 THz and the working temperature is 25 K. The electrons in injector level $1'$ are injected into the upper level 4 and then undergo vertical radiative and nonradiative transitions to the lower lasing level. Finally, electrons in the lower lasing level relax to level 1 through fast electron-longitudinal phonon scattering. This process then repeats in subsequent modules.

The band structure of this terahertz QCL is obtained by the self-consistent Poisson-Schrodinger equations which have been widely used to solve similar problems. The energy gap ε_{43} between level 4 and level 3 is 14.6 meV (3.7 THz) and ε_{42} is 19.4 meV (4.9 THz). The dipole matrix element d_{ab} can be calculated by the obtained wave functions.

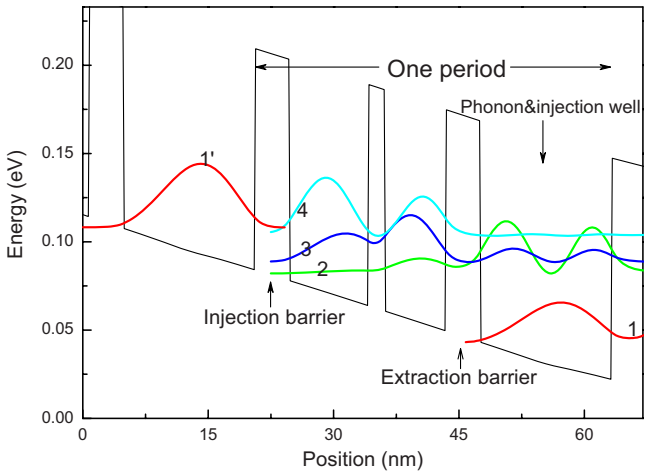

FIG. 1. (Color online) Calculated GaAs/$Al_{0.15}Ga_{0.85}As$ band structure of a portion of the active region and the relevant wave functions. The designed bias is 14.4 kV/cm. The layer thickness are **48**/96/**20**/74/**42**/161 Å, starting from the injector barrier with barriers indicated in bold fonts and doped layer (the center 36 Å of the 161 Å injector well is doped with Si to 10^{17} cm^{-3} to give a two-dimensional carrier concentration of 3.6×10^{10} cm^{-2} per module) underlined (Ref. 20).

We suppose the frequency of the pump-laser field which will be coupled into the QCL waveguide along the growth direction can be tunable from 2.5 to 4.25 THz. We consider a hyperbolic secant functional form for the initial far-IR pulse,[18] which described by

$$E_t = E_0 \sec h[1.76(t-t_0)/\tau_p]\cos[\omega(t-t_0)], \tag{1}$$

where E_0 is the electric-field amplitude, t_0 is the delay of the pulse, τ_p is the pulse duration, and ω is the pump frequency. In this paper, we set τ_p at 0.5 ps and t_0 at zero. In a useful pulse form, the pulse duration must be larger than the optical cycle $\tau_p > 2\pi/\omega$. The input pulse area is

$$\Theta = \int_{-\infty}^{\infty} \frac{d_{ab}}{\hbar} E_t dt = \Omega_0 \tau_p \pi / 1.76, \tag{2}$$

where $\Omega_0 = -d_{ab}E_0/\hbar$ is the peak of the Rabi frequency.

Although we have chose the pump frequency to be tunable, the polarization between levels 4 and 2 can be neglected in our equations because the dipole matrix element $d_{42}=2.23e$ Å is much smaller than $d_{43}=57.6e$ Å. With the averaging method, the effective Bloch equations have been used in the biased asymmetric quantum wells.[17] By appending the cascade term N_1/τ_{tunnel} to the original model, we make the electrons transport in a repeating mode and advance the following four-level effective Bloch equations:

$$\frac{d}{dt}P^{43} = -\frac{P^{43}}{\tau_{deph}} - \frac{i}{\hbar}[\varepsilon_{43} + \alpha_{43} - \gamma_{43}(N_4 - N_3)]P^{43} + \frac{i}{\hbar}(d_{43}E_t - 2\beta_{43}\,\mathrm{Re}\,P^{43})(N_4 - N_3),$$

TABLE I. The relaxation time (ps) derived from the results of MC simulation.

τ_{43}	τ_{42}	τ_{32}	τ_{31}	τ_{21}	τ_{tunnel}
31.7	33.5	13.5	2.9	0.98	20.8

$$\frac{d}{dt}N_4 = \frac{N_1}{\tau_{tunnel}} - \frac{N_4}{\tau_{43}} - \frac{N_4}{\tau_{42}} - \frac{2}{\hbar}(d_{43}E_t - 2\beta_{43}\,\mathrm{Re}\,P^{43})\mathrm{Im}\,P^{43},$$

$$\frac{d}{dt}N_3 = \frac{N_4}{\tau_{43}} - \frac{N_3}{\tau_{32}} - \frac{N_3}{\tau_{31}} + \frac{2}{\hbar}(d_{43}E_t - 2\beta_{43}\,\mathrm{Re}\,P^{43})\mathrm{Im}\,P^{43},$$

$$\frac{d}{dt}N_2 = \frac{N_4}{\tau_{42}} + \frac{N_3}{\tau_{32}} - \frac{N_2}{\tau_{21}},$$

$$\frac{d}{dt}N_1 = \frac{N_3}{\tau_{31}} + \frac{N_2}{\tau_{21}} - \frac{N_1}{\tau_{tunnel}}. \tag{3}$$

Here, P^{43} represents the mean polarizations between levels 4 and 3 per electron; N_1, N_2, N_3, and N_4 are the mean occupations of the population per electron at different levels; and τ_{ab} is the time of relaxation (related with the scattering rates) from level a to level b and τ_{tunnel} is the tunneling rate from level $1'$ of the last period to level 4 of this period. α_{43}, β_{43}, and γ_{43} represent the subband shift, the exchange correction, and the interplay between vertex and self-energy correction, respectively. These three items are induced by the Coulomb interaction[15] and can be described as

$$\alpha_{ab} = \frac{\pi e^2}{\epsilon} N_s \left(\frac{V_{aaaa} - V_{bbbb}}{2} \right),$$

$$\beta_{ab} = \frac{\pi e^2}{\epsilon} N_s V_{aabb},$$

$$\gamma_{ab} = \frac{\pi e^2}{\epsilon} N_s \left(V_{abba} - \frac{V_{aaaa} + V_{bbbb}}{2} \right). \tag{4}$$

The form factor of Coulomb matrix elements $V_{1,2,3,4} = \int\int dz dz' \phi_1(z)\phi_2(z')|z-z'|\phi_3(z')\phi_4(z)$, where ϕ_a is the wave function of subband a. Here, the dielectric constant ϵ is simply set at $12\epsilon_0$. N_s is the electron sheet density. The calculated parameters are listed in Tables I and II.

The intersubband energy gap was renormalized by the many-body items.[15] Here, the time-dependent transition energy is described as

$$\hbar\omega_{43}(t) = \varepsilon_{43} + \alpha_{43} - \gamma_{43}(N_4 - N_3) + \beta_{43}(N_4 - N_3). \tag{5}$$

TABLE II. The many-body items calculated by the wave functions obtained in the model (unit: J).

α_{43}	β_{43}	γ_{43}
-1.836×10^{-22}	-8.275×10^{-22}	4.137×10^{-22}

Here, the cascade method is as the same as the rate-equation model which have been used in Choi's letters[7,8] because the effective Bloch equations are derived with the averaging method. The tunneling mechanism between level $1'$ of the last period and level 4 can be approximately dealt using the scattering rate, just like how we disposed in MC simulation.[20] All the scattering rates we use in this paper are derived from the results of MC simulation in the stationary state and we suppose they fit the processes we deal with because the exiting time of the pump field is so short that the scattering rates make no change. The mean population occupations of the four levels in steady states are 0.417, 0.032, 0.014, and 0.537, so the population inversion between level 4 and level 3 in steady states is 0.385. The dephasing time of the polarization τ_{deph} is an important parameter that affects the polarized properties. This parameter cannot be calculated exactly and directly because it has a relation with many factors, such as the fabrication process and impurities. It will be discussed in the next section.

III. NUMERICAL RESULT

Although the Rabi flopping induced by a 2π Gaussian pulse in terahertz QCL has been studied,[12] the electron-electron scattering was not included and the many-body effects on population dynamics have not been investigated. In this section, we investigate the different simulation results with nonlinear chirped and nonchirped pulses, respectively.

A. Nonlinear chirped pulse case

The changes in population inversion in quantum wells induced by chirped pulse have been widely studied[16,17]and deeper change in population inversion can be induced by chirped pulse than that induced by nonchirped pulse.[17] The Rabi flopping can be achieved easily by using the designed chirped pump pulse. So, we choose the pump frequency to be nonlinear chirped which can be derived from Eq. (5) and set $\tau_{deph}=10$ ps. We clearly represent the evolution of the pump frequency of the nonlinear chirped pulse in Fig. 2(a). In the time of pulse duration, the pump frequency is rapidly rising. After the pulse quickly declines, the pump frequency changes in the recovery process. It is different with the result of asymmetric quantum wells because no recovery process happened in quantum wells.[16] In Fig. 2(b), we show the change in population inversion in the pump and recovery processes. In the pump process, the population inversion quickly declines to −0.3 and the Rabi flopping is achieved. We also find almost invisible oscillations in the insets of Fig. 2.

The population dynamics of the terahertz QCL pumped by a nonlinear chirped 2π pulse shown in Fig. 3(a) is investigated. As we know, the effective 2π pulse can make the population change back to the original situation. The simulation results with different dephasing times are shown in Figs. 3(b) and 3(c). In the pump process, we find the lowest population inversion is only −0.12. The change in population inversion is smaller than what we have observed in Fig. 2(b). With a dephasing time of 10 ps, we clearly find the obvious

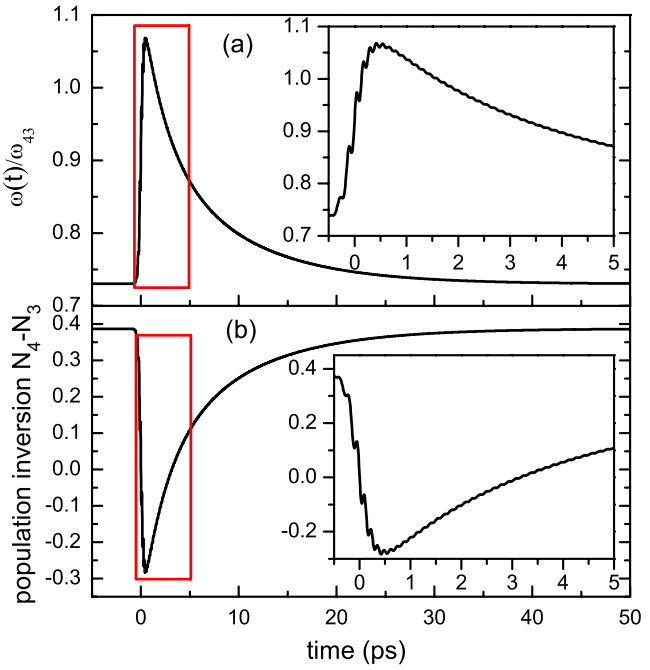

FIG. 2. (Color online) (a) The frequency of effective π pulse accounting for the time-dependent renormalized subband splitting. (b) The change in population inversion with a dephasing time of 10 ps. (The insets show details of time-dependent frequency and population inversion in the red rectangular frame.)

oscillations in recovery process in Fig. 3(b). The oscillations are shown in such a long time even when the electric field has already declined to almost zero. This phenomenon is the obvious evidence that the residual polarization also exerts an influence in the recovery process. In Fig. 3(c), the oscillations in recovery process disappear when we set the dephasing time at 1 ps because the residual polarization declines quickly. Comparing with the result in Fig. 2(b), we can observe more visible oscillations with an effective 2π pulse at the same dephasing time of 10 ps. From Eq. (2), the only difference between π pulse and 2π pulse is the electric-field amplitude. The larger electric field in 2π pulse makes the residual polarization stronger in the recovery process, so the phenomenon of oscillations can be observed more clearly in Fig. 3(b).

From the results described above, the coherent polarization makes a dominating effect in the pump process because the pump pulse duration is shorter than the relaxation time. The recovery process can be considered to be a superposition of the relaxation and the residual polarization. In addition, when we put forward the linear chirped pulse, we find the results have the same properties with the nonlinear chirped pulse.

B. Nonchirped pulse case

It is supposed that the pump pulse of 3.7 THz cannot be resonant with the energy gap between level 4 and level 3, so we put forward the nonlinear chirped pulse in last section. But it is difficult to control the pump frequency in such a short time scale. Now, we show the simulation results with

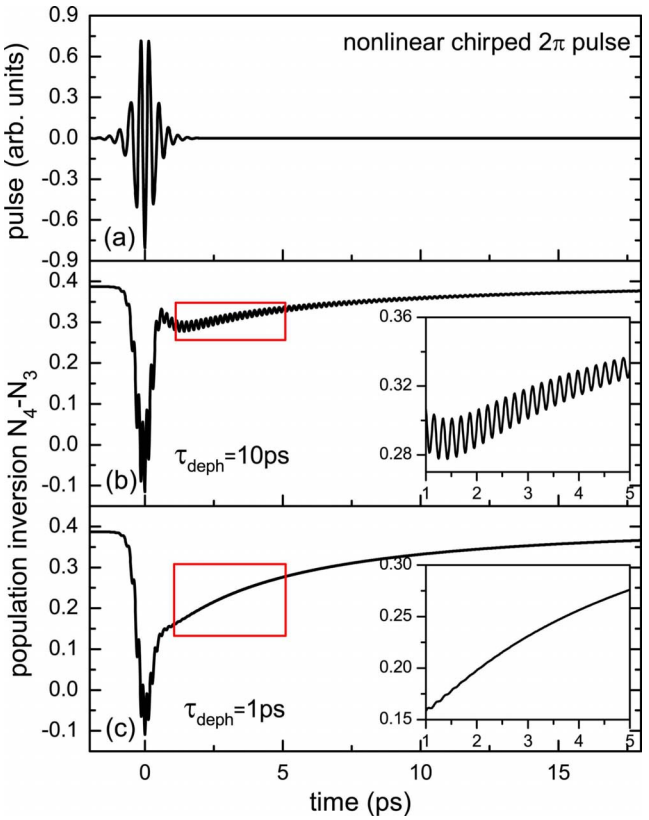

FIG. 3. (Color online) (a) The electric field of the effective time-dependent 2π pulse. (b) The change in population inversion induced by the pulse in (a) with a dephasing time of 10 ps. (c) Same as in (b) but with a dephasing time of 1 ps. (The insets show details of population inversion in the red rectangular frame.)

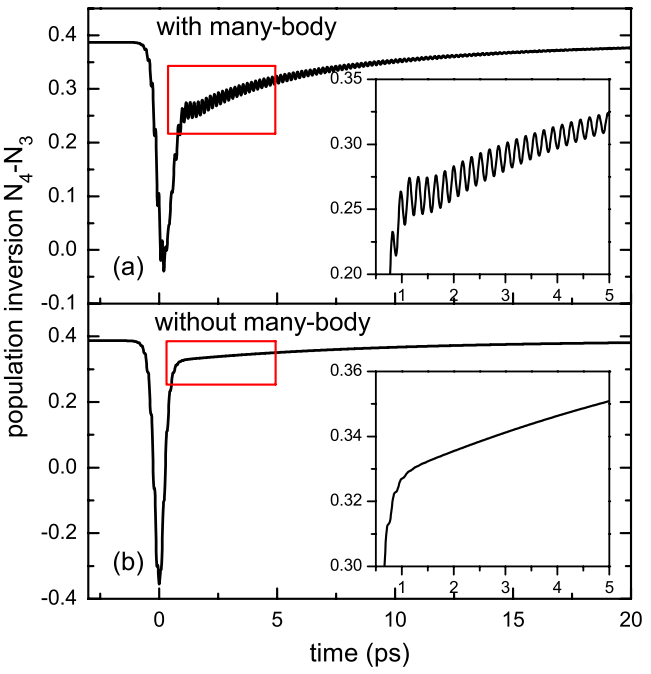

FIG. 4. (Color online) The change in population inversions induced by 2π pulse (a) with and (b) without the many-body effects. The pump frequency is 3.7 THz and the dephasing time is 10 ps. (The insets show details of population inversion in the red rectangular frame.)

the pump frequency fixed at 3.7 THz in Fig. 4. In order to compare with Fig. 3, we choose a 2π pulse.

With the many-body effects, we find the small flopping of population inversion and the oscillations in the recovery process in Fig. 4(a). In Fig. 4(b), we represent the simulated result when we set the many-body items α_{43}, β_{43}, and γ_{43} at zero and the smooth line in the recovery process is shown. Here, we can make an further explanation of the phenomenon we have observed in Fig. 3(b). The oscillations in recovery process are induced by the many-body effects of the polarization. In another word, the many-body items make the residual polarization affect the recovery process strongly. At the same time, compared with Fig. 3(b), we also find the lowest population inversion in the pump process is close to –0.36 in Fig. 4(b). So, the completed Rabi flopping can be induced without many-body effects.

It is well known that the recovery oscillations also can be induced by the polarization between subbands $1'$ and 4.[4] We did not take account of the polarization $P_{1'4}$ in the equations. But, to some extent, it can be good because we can distinguish the oscillations induced by the polarization $P_{1'4}$ from the oscillations induced by the many-body effects and our focus on the many-body effects can be emphasized. So, here we put forward another possible mechanism that causes the recovery oscillations in quantum cascade devices and accordingly show the importance of many-body effects in the device with long dephasing time. In order to find a new resonant pump frequency that can induce the largest flopping of population inversion with many-body effects, the figure of lowest population inversions caused by nonchirped π pulses with different pump frequencies is presented in Fig. 5(a).

In Fig. 5(a), we find the resonant pump frequency is 3.7 THz when we set the many-body items α_{43}, β_{43}, and γ_{43} at zero. With many-body effects, it is shown that the new largest flopping is happened at 3.15 THz which can be treated as the new resonant pump frequency. The red dot line in Fig. 5(a) is the simulation results when we set the many-body items β_{43} and γ_{43} at zero. From this figure, we find the many-body item α_{43} only makes the line shift compared with the black line without many-body effects, and the many-body items β_{43} and γ_{43} make the line inhomogeneously broaden besides bringing a shift of energy gap. We can understand this figure from Eq. (5) because the many-body items β_{43} and γ_{43} multiply the time-dependent population inversion and the many-body item α_{43} affects the energy gap directly. In Fig. 5(b), we present the change in population inversion when we choose the optimal pump frequency 3.15 THz and the visible oscillations in recovery process can be observed.

We choose the pump frequency of 3.15 THz on the new resonant condition and observe the population changes in four levels. From Ref. 11, to some extent, we got a credible value of the dephasing time 1 ps. But the device in the reference is very different from ours, so we took the dephasing time 1 ps here for reference only. The calculated pulse energy is 209 pJ. In Choi's letter,[7] a ultrafast pulse was pumped to an operating QCL and the numerical results were simply calculated in a rate-equation model. Here, we can make a

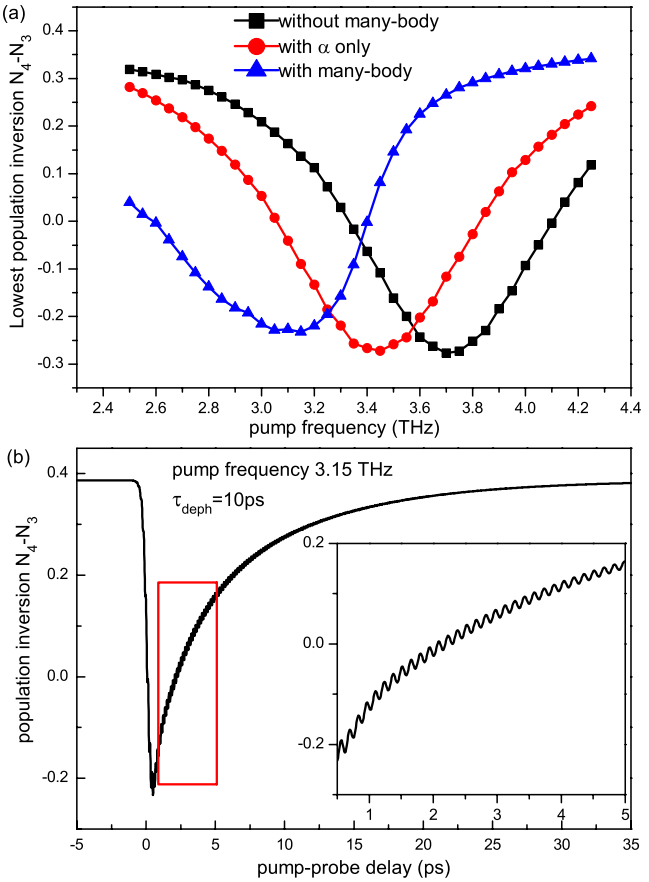

FIG. 5. (Color online) The lowest population inversions induced by the nonchirped π pulses with different pump frequencies. The lines represent the simulation results without many-body items (black ■), only with item α (red ●), and with all many-body items (blue ▲), respectively.

simple comparison. From Fig. 6, we can find the results have almost the same properties with the results of rate-equation model.[8] The smooth recovery process implies that the relaxation makes an dominating effect and the residual polarization can be neglected because the dephasing time is so short that the depolarization effect is strong. From the simulation results with different dephasing times, we find the oscillations totally disappear with the dephasing time of 2.5 ps approximately. In this point of view, we can find the practicability of the rate-equation model when the dephasing time is not that long.

IV. CONCLUSION

In conclusion, the properties of time-dependent population inversion with nonlinear chirped and nonchirped 2π and π pulses are reported. We demonstrate the feasibility of using the nonlinear chirped pulse to induce the almost total flopping of population inversion (from 0.38 to −0.3) in terahertz QCL. The nonchirped 3.7 THz pulse only induced little flopping (from 0.38 to −0.04) and the new resonant 3.15 THz pump pulse induced the flopping from 0.38 to −0.24. It is more efficient for the nonlinear chirped pulse to induce the flopping of population inversion. We also investigate the change in resonant pump frequency and the oscillations in recovery process, which both induced by the many-body effects in the polarization. These two phenomena accordingly show the importance of many-body effects in the devices with long dephasing time. The Rabi flopping and recovery of the population inversion can be obviously understood as gain flopping and gain recovery, so our results can be valuable for experiments on the operating terahertz QCL. In the terahertz QCL, the electron density is much smaller than that in mid-infrared QCL, so we think it will be more obvious of the oscillations in recovery process in mid-infrared QCL. At last, we observe the results of the population changes in four levels. We find it is similar as the results which were calculated with a rate-equation model. We figure that it is practicability to use the rate-equation model in a short dephasing time. In this paper, we find the cascade effective Bloch equations get an advantage over the rate-equation model although the computational complexity is almost the same since some interesting coherent phenomena induced by many-body effects can be observed by our theory.

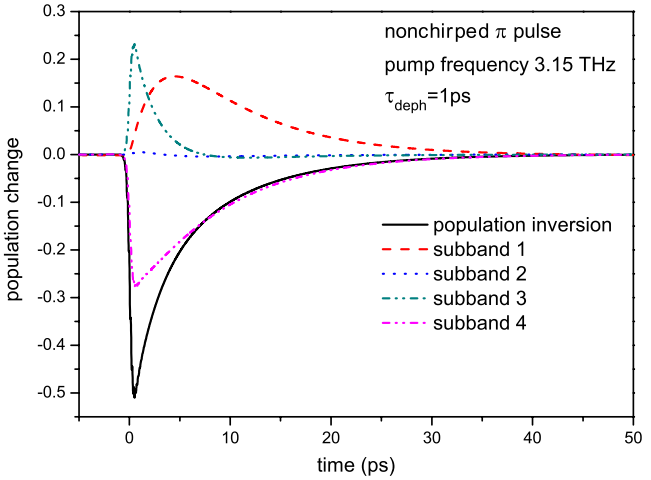

FIG. 6. (Color online) The population changes in four levels and the change in population inversion between level 4 and level 3 induced by nonchirped π pulse with the new resonant pump frequency of 3.15 THz. The dephasing time is 1 ps.

ACKNOWLEDGMENTS

We would like to thank H. Li for helpful discussions. This work was supported by the National Basic Research Program of China (Project No. 2007CB310402), the National Natural Science Foundation of China (Projects No. 60721004 and No. 60606027), and the major project (Project No. KGCX2-YW-231) and "Hundred Scholar Plan" of the Chinese Academy of Sciences.

*Author to whom correspondence should be addressed; jccao@mail.sim.ac.cn

[1] J. Faist, F. Capasso, D. L. Sivco, A. L. Hutchinson, and A. Y. Cho, Science **264**, 553 (1994).
[2] R. Köhler, A. Tredicucci, F. Beltram, H. E. Beere, E. H. Linfield, A. G. Davies, D. A. Ritchie, R. C. Iotti, and F. Rossi, Nature (London) **417**, 156 (2002).
[3] B. S. Williams, Nat. Photonics **1**, 517 (2007).
[4] F. Eickemeyer, K. Reimann, M. Woerner, T. Elsaesser, S. Barbieri, C. Sirtori, G. Strasser, T. Müller, R. Bratschitsch, and K. Unterrainer, Phys. Rev. Lett. **89**, 047402 (2002).
[5] R. C. Iotti and F. Rossi, Phys. Rev. Lett. **87**, 146603 (2001).
[6] C. Weber, A. Wacker, and A. Knorr, Phys. Rev. B **79**, 165322 (2009).
[7] H. Choi, T. B. Norris, T. Gresch, M. Giovannini, J. Faist, L. Diehl, and F. Capasso, Appl. Phys. Lett. **92**, 122114 (2008).
[8] H. Choi, L. Diehl, Z.-K. Wu, M. Giovannini, J. Faist, F. Capasso, and T. B. Norris, Phys. Rev. Lett. **100**, 167401 (2008).
[9] D. Indjin, P. Harrison, R. W. Kelsall, and Z. Ikonić, J. Appl. Phys. **91**, 9019 (2002).
[10] H. Li, J. C. Cao, J. T. Lü, and Y. J. Han, Appl. Phys. Lett. **92**, 221105 (2008).
[11] I. Waldmueller, W. W. Chow, E. W. Young, and M. C. Wanke, IEEE J. Quantum Electron. **42**, 292 (2006).
[12] C. Weber, F. Banit, S. Butscher, A. Knorr, and A. Wacker, Appl. Phys. Lett. **89**, 091112 (2006).
[13] I. Waldmueller, W. W. Chow, and A. Knorr, Phys. Rev. B **73**, 035433 (2006).
[14] A. A. Batista, P. I. Tamborenea, B. Birnir, M. S. Sherwin, and D. S. Citrin, Phys. Rev. B **66**, 195325 (2002).
[15] A. Olaya-Castro, M. Korkusinski, P. Hawrylak, and M. Yu. Ivanov, Phys. Rev. B **68**, 155305 (2003).
[16] A. A. Batista and D. S. Citrin, Phys. Rev. Lett. **92**, 127404 (2004).
[17] A. A. Batista and D. S. Citrin, Phys. Rev. B **74**, 195318 (2006).
[18] N. Cui, Y. Niu, H. Sun, and S. Gong, Phys. Rev. B **78**, 075323 (2008).
[19] H. Luo, S. R. Laframboise, Z. R. Wasilewski, G. C. Aers, H. C. Liu, and J. C. Cao, Appl. Phys. Lett. **90**, 041112 (2007).
[20] H. Li, Ph.D. thesis, Shanghai Institute of Microsystem and Information Technology, CAS, 2009.